Plasmonic/magnetic liposomes based on nanoparticles with multicore-shell architecture for chemo/thermotherapy

Ana Rita O. Rodrigues, Lia C. A. Santos, Daniela O. Macedo, Irina S. R. Rio, Ana Pires, André M. Pereira, João P. Araújo, Elisabete M. S. Castanheira and Paulo J. G. Coutinho

Physics Centre of Minho and Porto Universities (CF-UM-UP) and LaPMET Associate Laboratory, University of Minho, Campus of Gualtar, 4710-057 Braga, Portugal

ritarodrigues@fisica.uminho.pt

Abstract. Multifunctional nanosystems are capable to carry one or more therapeutic agents (thermal and/or targeting agents and chemotherapeutic drugs), offering the capability to concurrently perform different treatment modalities using a single nanosystem. Cluster nanostructures, consisting of densely packed aggregates of magnetic nanoparticles, have shown enhanced heating capabilities. Their combination with plasmonic nanoparticles enable synergistic behavior between dual hyperthermia (magneto-photothermia), allowing overheating cancer cells while increasing drug toxicity. In this work, multicore magnetic nanoparticles (NPs) of $MnFe_2O_4$ were prepared using oxamide and melamine as clustering agents. The multicore NPs prepared with oxamide were covered with a gold shell, resulting in multicore magnetic/plasmonic NPs with an increased SAR of 173.80 W/g, under NIR light. Liposomes based on these magnetic/plasmonic NPs were prepared and the model drug curcumin was loaded in these nanocarriers with a high encapsulation efficiency. The fusion between the curcumin-loaded magnetic/plasmonic liposomes and models of cell membranes (labelled with Nile Red) was confirmed by FRET, pointing the magneto/plasmonic liposomes as promising for dual cancer therapy (combined hyperthermia and chemotherapy).

1. Introduction

Hyperthermia is a type of therapy in which a tissue is heated to a higher temperature level, typically ranging from 41 ºC to 45 ºC. Its combination with chemotherapy has strong potential in treating advanced cancers, exhibiting a synergistic antitumor effect, better than the effect of monotherapy [1]. Yet, despite its potential, hyperthermia has struggled to be established as a therapeutic approach, because of its inadequate heat generation. Accordingly, the scientific community has been focused on the development of new nanomaterials with enhanced heating performance. Combining magnetic nanoparticles (NPs) with plasmonic gold nanoparticles (GNPs) has shown to provide a synergistic effect between the two local heating mechanisms [2-4].

$MnFe_2O_4$ nanoparticles are magnetic NPs of interest for their high magnetic susceptibility and chemical stability, and great heating efficiency [5,6]. Multicore magnetic nanoparticles, also known as colloidal clusters, are nanostructures with diverse applications in biomedicine and photonics. Cluster nanostructures have shown enhanced heating capabilities when compared to single NPs [7,8]. On the other hand, plasmonic NPs own large absorption cross section and can generate significant heat using

visible and/or NIR light. Gold is predominantly used as plasmonic metal for biomedical applications because of its biocompatibility, well-defined synthesis routes, resistance to oxidation, and flexible conjugation possibilities with organic molecules [9]. Due to its surface plasmon resonance effect, GNPs can greatly absorb light and because they have very low quantum emission efficiency, the absorbed radiation is converted into heat through a series of non-radiative decays (such as electron-electron and electron-phonon interactions), resulting in local heating of the NPs under electromagnetic radiation in the visible and near infra-red (NIR) range [10]. The NIR region between 650 nm and 950 nm, known as the first optical window, allows for deeper therapeutic depth in tissues than in the visible region due to a reduction in absorption.

Taking the hyperthermia potential of magnetic clusters, the enhanced heating effect of magnetic/plasmonic nanoarchitectures and the synergy between hyperthermia and chemotherapy, the development of sensitive liposomes containing multicore magnetic/plasmonic NPs is of extreme interest. This promising nanosystem allows the preservation of the magnetic and hyperthermia properties of the NPs, while providing suitable drug nanocarriers with improved drug pharmacokinetics.

2. Materials and methods

In all preparations, spectroscopic-grade solvents and ultrapure deionized water of Milli-Q grade (MilliporeSigma, St. Louis, MO, USA) were used.

2.1. Preparation of spherical $MnFe_2O_4$ nanoparticles

Spherical $MnFe_2O_4$ magnetic nanoparticles were prepared using the citrate stabilization method [11]. For that, 1 mmol of trisodium citrate dehydrate ($Na_3C_6H_5O_7$, 294.10 g/mol) and 0.47 mol of sodium hydroxide (NaOH, 18.9 M) were added to 19 mL of ultrapure water at 100 °C. Then, a 1 mL aqueous solution containing 1 mmol of iron sulphate ($FeSO_4$, 278.01 g/mol) and 0.5 mmol of manganese sulphate monohydrate ($MnSO_4.H_2O$, 169.02 g/mol) was added, drop by drop under stirring, to the previous solution. The reaction was maintained for 2 hours at 90 ºC, with magnetic stirring. After that, the obtained nanoparticles were washed with water and ethanol, in a 1:1 ratio, by magnetic decantation.

2.2. Synthesis of multicore magnetic NPs

Two types of multicore $MnFe_2O_4$ NPs were obtained using different aggregation agents, oxamide and melamine (figure 1). First, the hydroxyl groups of the $MnFe_2O_4$ NPs were activated by adding 2.2×10^{-4} mol of *N,N'*-carbonyldiimidazole (CDI) to 4.3×10^{-5} mol of the $MnFe_2O_4$ NPs dispersed in 25 mL of dry dimethyl sulfoxide. The solution was kept under sonication at 60 ºC, for 2 h. Then, the NPs were washed with water to eliminate the excess of CDI. Finally, the clustering agents were added in a molar ration of 1:2 (NPs:clustering agent) for oxamide, and 3:1 for melamine, taking into account their number of reaction sites. In order to promote a faster coupling between the amine groups of the clustering agents and the hydroxyl groups of the nanoparticles surface, imidazole was added (in the same molar ratio) and the reaction was kept at 60 ºC, for 2 h.

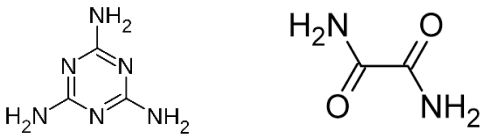

Figure 1. Chemical structure of melamine (left) and oxamide (right).

2.3. Synthesis of multicore magnetic/plasmonic NPs

For the synthesis of multicore magnetic/plasmonic NPs, gold nanoparticles were first prepared by the Brust-Schifrin method [12]. Briefly, 1.25 mL of 30 mM of gold (III) chloride hydrate was mixed with 4 mL of 50 mM of tetraoctylammonium bromide in toluene, acting as a phase-transfer reagent. Then, 1.25 mL of 0.4 M of sodium borohydride was slowly added, under magnetic stirring. After purification by washing with water, the gold NPs were coupled to the surface of the $MnFe_2O_4$ cluster (oxamide) for the growth of the shell. For that, cysteamine was added (at 5-fold molar excess to NPs quantity), to act as bridge between the hydroxyl surface groups of multicore $MnFe_2O_4$ NPs, while the remaining thiol provide strong chemisorption sites for gold nanoparticles. After 1 h at 60 ºC, washing by magnetic separation was performed to remove the gold NPs that were not attached to the surface of the multicore structures. Finally, the gold shell growth was promoted by the "seeding" method [13], in which the gold NPs coupled in the surface of the multicore manganese ones were used for the growth and coalescence of the gold shell. Briefly, to 2 mL of the multicore $MnFe_2O_4$ NPs decorated with gold NPs, 2.4 mL of $HAuCl_4$ (1%) and 2 mL of 40 mM of hydroxylamine were added. The final multicore magnetic/plasmonic NPs were washed by centrifugation, with water.

2.4. Preparation of aqueous liposomes containing multicore magnetic/plasmonic NPs

For the preparation of aqueous liposomes (magnetic/plasmonic liposomes) of $MnFe_2O_4$ clusters (oxamide) with gold shell, the lipid dipalmitoylphosphatidylcholine (DPPC) was used. For that, a 10 mM lipid solution in ethanol was injected, under vigorous vortexing, to an aqueous solution of 0.02 mg of the multicore magnetic/plasmonic NPs, above the melting transition temperature of the lipid DPPC (ethanolic injection method [14]). The final ferrofluid was purified by magnetic decantation and washed with water, to remove all the non-encapsulated NPs.

2.5. Preparation of model of membranes

Giant unilamellar vesicles (GUVs) were used as models of cell membranes [15]. First, a thin film of 1 mM of soy lecithin was pre-hydrated with 60 µL of ultrapure water and incubated at 45 °C, for 30 min. Then, 5 mL of a 0.1 M glucose aqueous solution was added and the solution was kept at 37 °C, for 2 h. After incubation, the suspension was centrifuged at 14,000 g for 30 min, to remove multilamellar vesicles and lipid aggregates.

2.6. Characterization techniques

The UV-Vis-NIR spectrophotometer Shimadzu UV-3600 Plus was used to record the absorption spectra. Fluorescence measurements were performed using a Fluorolog 3 spectrofluorimeter, equipped with double monochromators in both excitation and emission.

The hydrodynamic diameter, zeta potential value and polydispersity index were measured using Litesizer 500, a DLS instrument from Anton Paar, using a semiconductor laser diode of $\lambda = 658$ nm and 40 mW. Each sample was measured three times, at room temperature, and the experimental data were processed using Kalliope software.

The microscopy images were recorded using a Scanning Electron Microscopy, model NanoSEM-FEI Nova 200 in transmission mode (STEM).

The magnetic characterization was performed using a superconducting quantum interference device (SQUID) magnetometer MPMS3 (Quantum Design Inc., San Diego, CA, USA), operating with an applied magnetic field up to 4 T.

2.7. Measurement of the photothermal effect

The heating performance of the nanoparticles in solution was evaluated in a home-made setup, consisting of a continuous laser with a wavelength (808 nm, 1 W laser output power and a fluence of 1 W/cm^2) and a T-type thermocouple connected to a digital multimeter (Agilent U1242A) for temperature measurement. The temperature was recorded during 30 minutes of irradiation, plus 30 minutes of cooling (laser off).

3. Results and Discussion

3.1. Multicore magnetic/plasmonic NPs characterization

The UV-visible absorption spectra of the synthesized $MnFe_2O_4$ NPs and multicore nanostructures prepared with oxamide and melamine are displayed in figure 2. For comparison purposes, the mass concentration of the nanoparticles and clusters was certified to be the same. As expected, a wide absorption was observed for the $MnFe_2O_4$ nanoparticles, with a band at around 375 nm, in accordance with the previous observed for this type of NPs [11]. The higher absorption of the cluster nanostructures prepared with oxamide and melamine is consistent with a size increase, indicating the formation of large aggregates. In addition, the difference in light scattering in the range between 300 nm to 450 nm of the multicore nanostructures allow to anticipate the formation of different nanostructures.

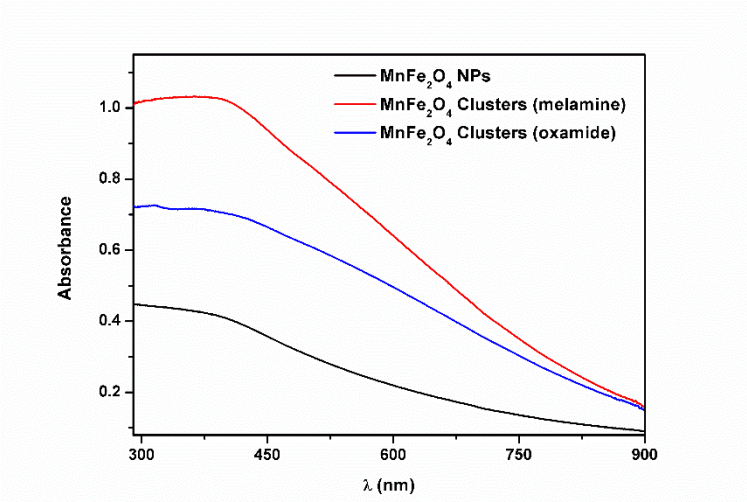

Figure 2. UV–visible absorption spectra of aqueous dispersions of $MnFe_2O_4$ NPs and $MnFe_2O_4$ clusters prepared with oxamide and melamine.

The electronic microscopy measurements of $MnFe_2O_4$ NPs and $MnFe_2O_4$ clusters enable the assessment of their size and shape and the obtained images are shown in figure 3. A homogeneous population of $MnFe_2O_4$ NPs with spherical shape was obtained by the co-precipitation method (figure 3-A and B), with sizes between 65.5 nm and 104.9 nm. On the other hand, roughly spherical nanostructures containing NPs aggregates were observed for the $MnFe_2O_4$ clusters (figure 3 – C and D). Larger aggregates were obtained for the $MnFe_2O_4$ clusters prepared with the clustering agent oxamide. On the other hand, the higher contrast of the $MnFe_2O_4$ clusters prepared with melamine indicate the formation of more dense aggregates with higher number of NPs packed per volume.

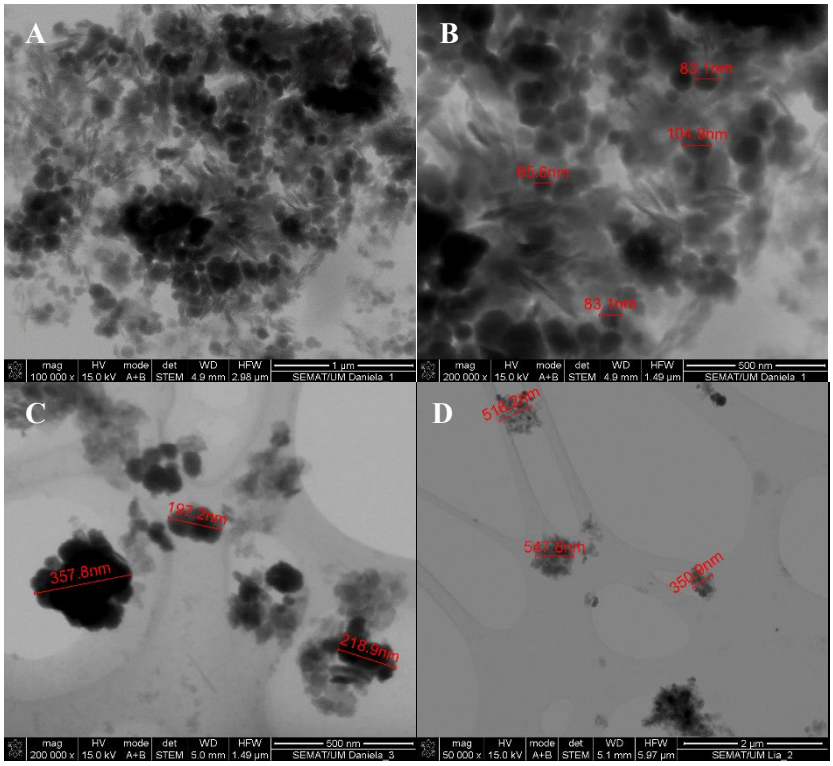

Figure 3. STEM images of: (A and B) $MnFe_2O_4$ NPs, (C) $MnFe_2O_4$ clusters (melamine) and (D) $MnFe_2O_4$ clusters (oxamide).

The magnetic properties of the $MnFe_2O_4$ clusters prepared with oxamide and melamine were evaluated by measuring their hysteresis loop at room temperature (figure 4). The M(H) curve of the $MnFe_2O_4$ NPs is shown for comparison. The obtained values of coercivity (C), remnant magnetization (M_R), saturation magnetization (M_S) and ratio between remnant magnetization and saturation magnetization (M_R/M_S) are summarized in Table 1.

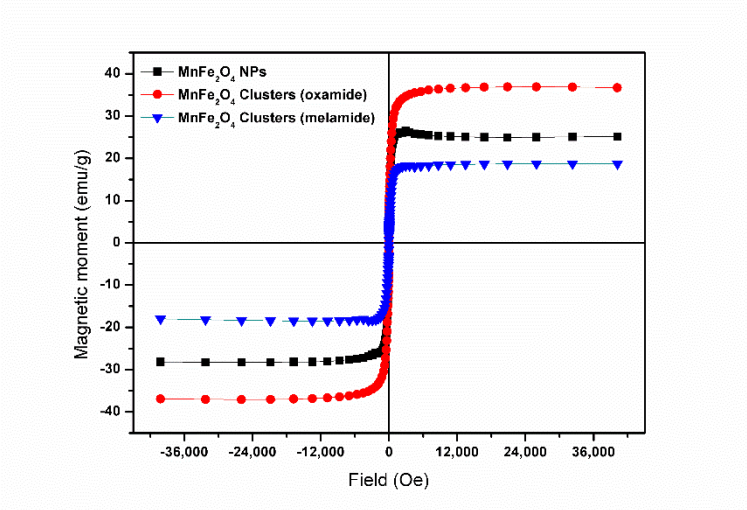

Figure 4. Hysteresis curve of the $MnFe_2O_4$ NPs, $MnFe_2O_4$ clusters (melamine) and $MnFe_2O_4$ clusters (oxamide), at room temperature.

Table 1. Values of coercivity (C), remnant magnetization (M_R) and saturation magnetization (M_S) and ratio between remnant magnetization and saturation magnetization (M_R/M_S), obtained from the hysteresis curve.

	M_S (emu/g)	M_R (emu/g)	M_R/M_S	C (Oe)
$MnFe_2O_4$ NPs	24.84	7.62	0.31	31.63
$MnFe_2O_4$ clusters (melamine)	18.45	3.03	0.16	27.17
$MnFe_2O_4$ clusters (oxamide)	37.41	7.79	0.21	5.01

A decrease of the saturation magnetization was observed for the clusters prepared with melamine as aggregation agent, while the opposite was observed for the clusters synthesized with oxamide. In fact, the magnetic behavior of multicore nanostructures is complex and it depends both on the sizes of their building blocks, i.e., single nanoparticles, and their final structure [16]. A similar behavior of magnetization decrease was previously observed for flower-shaped $MnFe_2O_4$ nanostructures, using melamine as cross-linking agent. In that work, the poor saturation magnetization of 6.16 emu/g was attributed to a weak internal ordering of the aggregates resulting in coupling of the spins of the cores within the multicore structures and dipole–dipole interactions of the clusters [11]. Nonetheless, the $MnFe_2O_4$ clusters prepared here with melamine show a higher saturation magnetization of 18.45 emu/g (table 1). On the other hand, an increase in the saturation magnetization was observed for the $MnFe_2O_4$ clusters prepared with oxamide, which can be attributed to better oriented cores within the aggregates. Despite the low values of remnant magnetization and coercivity, both nanostructures show a ferromagnetic behaviour with a M_R/M_S higher than 0.1 (which is the higher limit for superparamagnetism). Even so, it is worth notice that both cluster nanostructures have shown a decrease in the M_R/M_S ratio, indicating that these aggregate nanostructures lose more easily their magnetism upon field removal, comparing to single NPs.

Taking the better magnetic properties of the $MnFe_2O_4$ clusters prepared with oxamide, these nanostructures were selected for the synthesis of the multicore magnetic/plasmonic NPs. The UV-visible absorption spectrum of the $MnFe_2O_4$ clusters prepared with oxamide with the gold shell is shown in figure 5. The absorption spectrum of the $MnFe_2O_4$ clusters is shown for comparison. The increase in the range between 300 and 400 nm is consistent with an increase in size, while the absorption around 600 nm corroborates the formation of the gold shell. A higher photothermal effect is anticipated for the multicore magnetic/plasmonic NPs, under irradiation at 808 nm, due to its higher absorption at this wavelength.

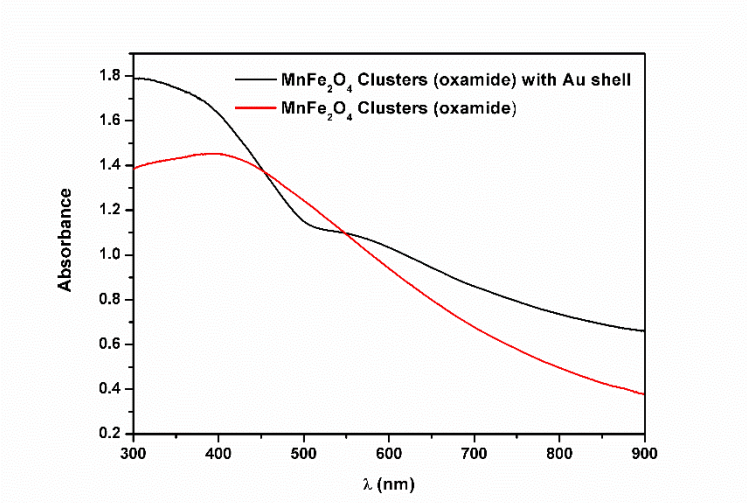

Figure 5. UV–visible absorption spectra of aqueous dispersions of $MnFe_2O_4$ clusters and $MnFe_2O_4$ clusters with Au shell.

The photothermal performance of the NPs was evaluated in aqueous solution (1 mg/mL) under NIR irradiation (808 nm) with a power density of 1 W/cm^2. To quantify and compare heating efficiencies of the magnetic NPs, multicore NPs and multicore magnetic/plasmonic NPs, their Specific Absorption Rate (SAR) was calculated using equation (1) [17].

$$SAR = \frac{m_W \times C_W}{m_P} \times \frac{\Delta T}{\Delta t} \quad (1)$$

where m_W and C_W corresponds, respectively, to the mass and specific heat capacity of the liquid media (water, C_W = 4.18 Jg^{-1}K^{-1}) and the component $\frac{\Delta T}{\Delta t}$ is the initial slope. The temperature variation and the obtained SAR values are summarized in table 2. Great values of SAR were obtained for the $MnFe_2O_4$ NPs, $MnFe_2O_4$ clusters and multicore magnetic/plasmonic NPs. An enhanced SAR value was both observed for the cluster and magnetic/plasmonic nanostructures. The highest SAR value of 173.8 Wg^{-1} was obtained for the $MnFe_2O_4$ clusters (oxamide) with gold shell, indicating that this nanoarchitectures are the most promising as heating agents for hyperthermia.

Table 2. Temperature variation (ΔT_{Max}), initial slope, mass and SAR value.

	ΔT_{Max} (°C)	**Initial Slope**	**Mass (mg)**	**SAR (Wg^{-1})**
$MnFe_2O_4$ NPs	15.3	0.0445	3.237	114.93
$MnFe_2O_4$ clusters (oxamide)	17.3	0.0498	3.237	128.62
$MnFe_2O_4$ clusters (oxamide) with gold shell	13.1	0.0390	1.876	173.80

Keeping in mind the synergistic effect between hyperthermia and controlled drug delivery, aqueous liposomes (magnetic/plasmonic liposomes) based on multicore magnetic/plasmonic NPs were prepared. The model drug curcumin was loaded into aqueous liposomes of $MnFe_2O_4$ clusters (oxamide) with gold shell. Aiming at a temperature-sensitive release of curcumin under NIR light, the lipid DPPC, with a transition temperature at 41 ºC, was used. The fluorescence emission of the curcumin encapsulated in neat liposomes (without nanoparticles) and magnetic/plasmonic liposomes was measured and the results are presented in figure 6. The size, surface charge and polydispersity index (PDI) of the magnetic/plasmonic liposomes were measured by DLS. The results are shown in table 3 and values for neat liposomes are presented for comparison.

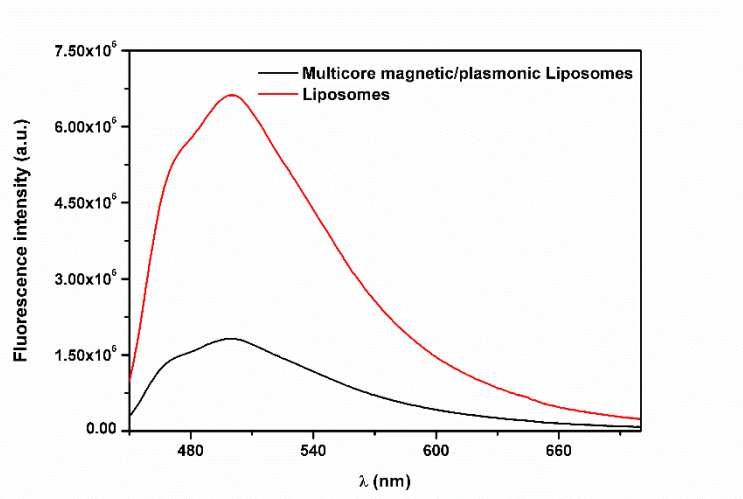

Figure 6. Emission spectra of curcumin (λ_{exc}= 440 nm) loaded in neat liposomes and liposomes containing $MnFe_2O_4$ clusters (oxamide) with gold shell.

Table 3. Mean values and standard deviation of hydrodynamic diameter, zeta potential and polydispersity index (PDI) of liposomes and Magnetic/plasmonic liposomes based on multicore magnetic/plasmonic NPs, obtained by DLS

	Hydrodynamic size ± SD (nm)	**Zeta Potential ± SD (mV)**	**PDI**
Liposomes	118.62 ± 6.89	-9.64 ± 0.76	0.26
Magnetic/plasmonic liposomes of $MnFe_2O_4$ clusters (oxamide) with gold shell	353.46 ± 19.81	-2.16 ± 1.03	0.28

An emission quenching by the nanoparticles is observed for curcumin in the magnetic/plasmonic liposomes (figure 6), confirming its encapsulation in the developed nanosystems. Multicore magnetic/plasmonic liposomes with hydrodynamic sizes of 353.46 ± 19.81 nm were obtained, being suitable for an enhanced permeability and retention effect (EPR) in tumor tissues [18]. The PDI values below 0.3 indicate a homogenous population and the almost neutral zeta potential is in accordance with the expected for the zwitterionic lipid DPPC. A high encapsulation efficiency (EE%) of 99.5% was obtained using the equation $EE(\%) = \frac{C_{total} - C_{non-encapsulated}}{C_{total}} \times 100$, indicating that the prepared multicore magnetic/plasmonic liposomes are ideal for the encapsulation and transport of the model drug curcumin.

The non-specific interaction of the synthesized nanosystems with models of cell membranes (GUVs) was evaluated by FRET (Förster Resonance Energy Transfer) [19,20]. For that, the fluorescence spectra of multicore magnetic/plasmonic liposomes containing the model drug curcumin (acting as energy donor), GUVs containing the hydrophobic probe Nile Red (acting as energy acceptor) and a mixture of both was measured exciting only the donor (λ_{exc}= 440 nm). The results of this study are shown in figure 7.

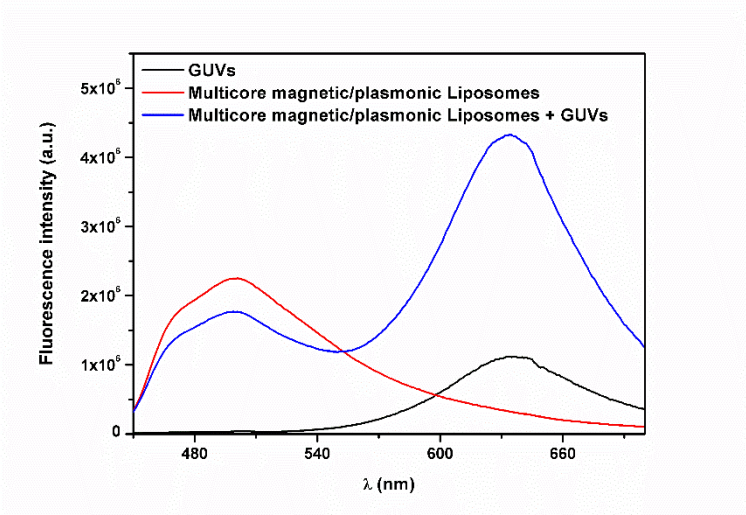

Figure 7. Emission spectra (λ_{exc}= 440 nm) of GUVs containing Nile Red, Liposomes of multicore magnetic/plasmonic NPs containing only curcumin, and mixture of both.

As expected, a typical curcumin emission band was observed around 500 nm for multicore magnetic/plasmonic liposomes containing only the donor, while residual fluorescence was observed for the GUVs containing Nile Red. After mixing the GUVs (labelled with Nile Red) with the curcumin-

loaded liposomes containing multicore magnetic/plasmonic NPs, if membrane fusion occurs, the energy transfer between curcumin and Nile Red will be promoted by the closer proximity between the donor acceptor. The observed decrease in the first band corresponding to the curcumin emission and increase in the second corresponding to the Nile Red, is caused by the energy transfer of the excited curcumin molecules. Hence, the observed decrease in the donor emission and increase in the acceptor band after interaction with GUVS is consistent with FRET and confirms the membrane fusion between the two systems.

4. Conclusion

Magnetic multicore NPs, consisting of densely packed aggregates of manganese ferrite, were prepared using melamine and oxamide as clustering agents. The $MnFe_2O_4$ clusters synthesized with oxamide have shown an enhanced magnetization of 37.41 emu/g, compared to single NPs. These nanostructures were covered with a gold shell and their photothermal potential was evaluated, showing a temperature variation increase of 13.1º C under NIR light (during 30 min). This NPs were incorporated in liposomes together with the drug model curcumin, resulting in magnetic/plasmonic liposomes. Their fusion with models of cell membrane was confirmed by FRET. Hence, the prepared nanosystems are promising for the encapsulation and controlled release of curcumin, while being potential as photothermal agents.

5. References

[1] Phung, D.C., Nguyen, H.T., Phuong Tran, T.T. (2019) Combined hyperthermia and chemotherapy as a synergistic anticancer treatment. J. Pharm. Investig. 49, 519–526. DOI:10.1007/s40005-019-00431-5

[2] Ovejero, J.G., Morales, I., Presa, P., Mille, N., Carrey, J., Garcia, M. A., Hernando, A., Herrasti, P. (2018) Hybrid nanoparticles for magnetic and plasmonic hyperthermia. Phys. Chem. Chem. Phys. 20, 24065-24073. DOI:10.1039/C8CP02513D

[3] Cortes, E.C., Cabana, S., Boitard, C., Zehlig, E., Griffete, N., Fresnais, J., Wilhelm, C., Hassan, A.A., Ménager, C. (2019) Recent insights in magnetic hyperthermia: From the "hot-spot" effect for local delivery to combined magneto-photo-thermia using magneto-plasmonic hybrids. Adv. Drug Del. Rev. (138) 233-246. DOI:10.1016/j.addr.2018.10.016. DOI: 10.1039/C9NH00332K

[4] Tymoczko, A., Kamp, M., Rehbock, C., Kienle, L., Cattaruzza, E., Barcikowski, S., Amendola, V. (2019) One-step synthesis of Fe–Au core–shell magnetic-plasmonic nanoparticles driven by interface energy minimization. Nanoscale Hor. 4, 1326-1332.

[5] Rodrigues, A.R.O., Ramos, J.M.F., Gomes, I.T., Almeida, B.G., Araújo, J.P., Queiroz, M.-J.R.P., Coutinho, P.J.G., Castanheira, E.M.S. (2016) Magnetoliposomes based on manganese ferrite NPs as nanocarriers for antitumor drugs. RSC Adv. 6, 17302–17313. DOI: 10.1039/C5RA27058H

[6] Deng, K, Chen, Y., Li, C., Deng, X., Hou, Z., Cheng, Z., Han, Y., Xing, B., Lin, J. (2017) 808 nm light responsive nanotheranostic agents based on near-infrared dye functionalized manganese ferrite for magnetic-targeted and imaging-guided photodynamic/photothermal therapy. J. Mater. Chem. B. 5, 1803-1814. DOI:10.1039/C6TB03233H

[7] Huang, Chih-C., Chang, Po-Y., Liu, CHien-L., Xu, Jia-P., Wu, Shu-P., Kuo, Wen-C. (2015) New insight on optical and magnetic Fe_3O_4 nanoclusters promising for near infrared theranostic applications. Nanoscale, 7, 12689-12697. DOI:10.1039/C5NR03157

[8] Estorozhuk, L., Besenhard, M.O., Mourdikoudis, S., LaGrow, A.P., Lees, M.R., Tung, L.D., Gavriilidis. A., Thanh. N.T.K. (2021) Stable Iron Oxide Nanoflowers with Exceptional Magnetic Heating Efficiency: Simple and Fast Polyol Synthesis. ACS Applied Materials & Interfaces 13, 45870-45880. DOI: 10.1021/acsami.1c12323

[9] Elahi, N., Kamali, M., Baghersad, M. H. (2018) Recent biomedical applications of gold

nanoparticles: A review. Talanta 184, 537-556. DOI:10.1016/j.talanta.2018.02.088
[10] Zeng, N., Murphy, A. B. (2009) Heat generation by optically and thermally interacting aggregates of gold nanoparticles under illumination. Nanotechnology 20, 375702. DOI: 10.1016/j.talanta.2018.02.088
[11] Lopes, F.A.C., Fernandes, A.V.F., Rodrigues, J.M., Queiroz, M.-J.R.P., Almeida, B.G., Pires, A., Pereira, A.M., Araújo, J.P., Castanheira, E.M.S., Rodrigues, A.R.O., Coutinho, P.J.G. (2022) Magnetoliposomes Containing Multicore Nanoparticles and a New Antitumor Thienopyridine Compound with Potential Application in Chemo/Thermotherapy. Biomedicines 10, 1547. DOI: 10.3390/biomedicines10071547
[12] Rio, I.R.S., Rodrigues, A.R.R., Rodrigues, J.M., Queiroz, M.J.R.P., Calhelha, R.C., Ferreira, I.C.F.R., Almeida, B.G., Pires., A.. Pereira, A.M., Araújo, J.P., Castanheira, E.M.S., Coutinho,. P.J.G, (2021) Magnetoliposomes Based on Magnetic/Plasmonic Nanoparticles Loaded with Tricyclic Lactones for Combined Cancer Therapy. Pharmaceutics 13(11), 1905. DOI:10.3390/pharmaceutics13111905
[13] Brown, K.R., Natan, M.J. (1998) Hydroxylamine seeding of colloidal Au nanoparticles in solution and on surfaces. Langmuir 14, 726–728. DOI: 10.1021/la970982u
[14] Ribeiro, B.C., Alvarez, C.A.R., Alves, B.C., Rodrigues, J.M., Queiroz, M.J.R.P., Almeida, B.G., Pires, A., Pereira, A.M., Araújo, J.P., Coutinho, P.J.G., Rodrigues, A.R.O., Castanheira, E.M.S. (2022) Development of Thermo- and pH-Sensitive Liposomal Magnetic Carriers for New Potential Antitumor Thienopyridine Derivatives. Materials 15, 1737. DOI:10.3390/ma15051737
[15] Tamba, Y., Terashima, H., Yamazaki, M. (2011) A Membrane Filtering Method for the Purification of Giant Unilamellar Vesicles. Chem. Phys. Lipids 164, 351–358. DOI: 10.1016/j.chemphyslip.2011.04.003
[16] Storozhuk, L., Besenhard, M.O., Mourdikoudis, S., LaGrow, A.P., Lees, M.R., Tung, L.D., Gavriilidis, A., Thanh, N.T.K. (2021) Stable Iron Oxide Nanoflowers with Exceptional Magnetic Heating Efficiency: Simple and Fast Polyol Synthesis. ACS Appl. Mater. Interfaces 13, 45870–45880. DOI:10.1021/acsami.1c12323
[17] Espinosa, A., Tabi, J. K., Hassan, A. A., Sangnier, A. P., Curcio, A., Silva, A. K. A. Corato, R., Neveu, S., Pellegrino, T, Marzan, L., Wilhelm, C. (2018) Magnetic (hyper)thermia or photothermia? progressive comparison of iron oxide and gold nanoparticles heating in water, in cells, and in vivo. 28, 1803660. DOI: 10.1002/adfm.201803660
[18] Kang, H., Rho, S., Stiles, W.R., Hu, S., Baek, Y., Hwang, D.W., Kashiwagi, S., Kim, M.S., Choi, H.S. (2020) Size-Dependent EPR Effect of Polymeric Nanoparticles on Tumor Targeting. Adv. Healthc. Mater. 9, e1901223. DOI: 10.1002/adhm.201901223
[19] Cardoso, B.D., Rodrigues, A.R., Almeida, B.G., Amorim, C.O., Amaral, V.S., Castanheira, E.M.S., Coutinho, P.J.G. (2020) Stealth Magnetoliposomes Based on Calcium-Substituted Magnesium Ferrite NPs for Curcumin Transport and Release. Int. J. Mol. Sci. 21, 3641. DOI: 1422-0067/21/10/3641
[20] Rio, I.S.R., Rodrigues, A.R.O., Rodrigues, C.P., Almeida, B.G., Pires, A., Pereira, A.M., Araújo, J.P., Castanheira, E.M.S., Coutinho, P.J.G. (2020) Development of Novel Magnetoliposomes Containing Nickel Ferrite Nanoparticles Covered with Gold for Applications in Thermotherapy. Materials 13, 815. DOI:10.3390/ma13040815